ARTICLES

Radial response of individual bubbles subjected to shock wave lithotripsy pulses *in vitro*

Thomas J. Matula and Paul R. Hilmo
Applied Physics Laboratory, Center for Industrial and Medical Ultrasound, University of Washington, Seattle, Washington 98105

Brian D. Storey
Franklin W. Olin College of Engineering, Needham, Massachusetts 02492

Andrew J. Szeri
Department of Mechanical Engineering, University of California, Berkeley, California 94720-1740

(Received 12 July 2001; accepted 16 November 2001)

Direct measurements of individual bubble oscillations in lithotripsy fields have been performed using light-scattering techniques. Studies were performed with bubble clouds in gassy water as well as single levitated bubbles in degassed water. There is direct evidence that the bubble survives the inertial collapse, rebounding several times before breaking up. Bubble dynamics calculations agree well with the observations, provided that vapor trapping (a reduction in condensation during bubble collapse) is included. Furthermore, the afterbounces are dominated by vapor diffusion, not gas diffusion. Vapor trapping is important in limiting the collapse strength of bubbles, and in sonochemical activity. © *2002 American Institute of Physics.* [DOI: 10.1063/1.1433970]

I. INTRODUCTION

Every year, over 100 000 people are treated for kidney stones in the United States, and many times that worldwide. In 1990, about 85% of these patients[1] were treated with shock wave lithotripsy (SWL),[2] a method in which high intensity shock waves are focused at the site of the stone, resulting in stone comminution. Despite the widespread use of SWL, there is no agreement in the literature as to the mechanism by which the shock wave destroys kidney stones. Possible contributors include spallation,[3] direct acoustic shearing of the stone,[4] fatigue,[5] focused stress waves,[6] cavitation,[7–9] and most recently, squeezing.[10] Furthermore, although early reports indicated that SWL treatment did not lead to appreciable damage to the kidney, it is now recognized that a clinical dose (≈2000 shock waves) will induce renal injury in a majority, if not all, treated kidneys.[11]

In an electrohydraulic lithotripter (Fig. 1), the shock wave generated by an underwater explosion at the internal focus (F1) of an ellipsoidal reflector is focused on the kidney stone at the external focus (F2). Typical *in vitro* measurements of the shock wave in water indicate that at F2, a 40 MPa, 1-μs compression is followed by a -10 MPa, 5 μs rarefaction (the *spatial* profile is shown in the inset of Fig. 1).[12] The -6 dB region is cigar-shaped and roughly 6 cm long by 1 cm in diameter.[13]

It is commonly accepted that the initial compression wave compresses preexisting bubbles. The rarefaction following the shock then causes these micro-bubbles to grow to millimeter dimensions before collapsing inertially after hundreds of microseconds. Acoustic emission detected *in vivo* agrees with these long growth and collapse cycles.[14] Accordingly, acoustic cavitation has been an important area of research on the mechanisms for stone comminution (as well as tissue damage) in SWL.

The SWL cavitation field has been characterized with acoustic techniques,[14–17] foils,[17] high-speed video,[17–19] and recently with laser illumination.[20,21] In particular, acoustic detection of bubble emissions have proved useful in verifying bubble dynamics equations for modeling the radius-time, or $R(t)$ of bubbles subjected to SWL pulses. Currently most formulations of bubble dynamics associated with SWL use the Gilmore model.[22] Figure 2 illustrates the success of the model in matching the time interval t_C between acoustic signals from the forced compression and inertial collapse.

Although indirect methods for measuring $R(t)$ dynamics have proved useful for many applications, they are not a direct measure of bubble dynamics, and do not provide a complete understanding of bubble motion. High-speed movies do provide some information as to the radial motion, but only over very short times when the bubble is large enough to be observed, and at a very high cost. Hence, a more direct measurement of bubble motion that can detect smaller bubbles in real time, over their complete motion, is desired.

In this paper we examine the detailed dynamics associated with bubbles subjected to a SWL pulse with experiments and theory. Light-scattering techniques are employed to measure the $R(t)$ curve of *single* bubbles in the SWL cavitation field. The experiments described here differ from previous research using light-scattering from bubbles in SWL[20] in that we measure the instantaneous (nonaveraged)

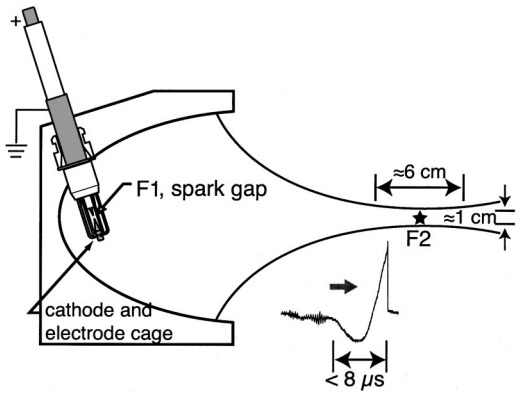

FIG. 1. A diagram of the electrohydraulic shock wave lithotripter (SWL). A spark discharge located at the first focus of an ellipsoidal reflector is reflected by the ellipsoid and focused at the second focus, F2. The *spatial* profile of a measured shock wave is also shown.

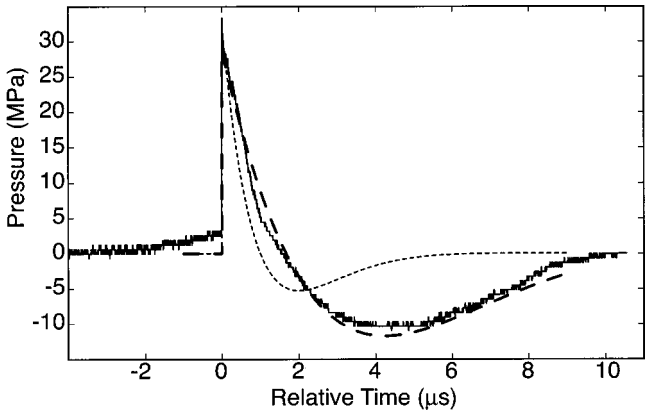

FIG. 3. Comparison of theoretical shock wave of Eq. (1) (short dashed line) and our artificially extended measured shock wave (solid line), together with our new fitting parameters (long dashed line), $\alpha = 3.5\times10^5$ and $f = 50.0$ kHz.

response from individual bubbles, not from bubble clouds. The measurements show that the rebounds, or afterbounces, of the bubble can be matched to numerical simulations only when water vapor and heat transfer are included in the simulations. The addition of water vapor in the simulations dramatically affects the bubble dynamics, as well as the hot-spot conditions that exist in the collapsed bubble.

The paper is organized as follows: First, the acoustic wave generated by SWL is reviewed, followed by a theoretical description of the model used to calculate spherical bubble dynamics. The experimental system and results follow, and comparisons with the model are made. Implications are then discussed.

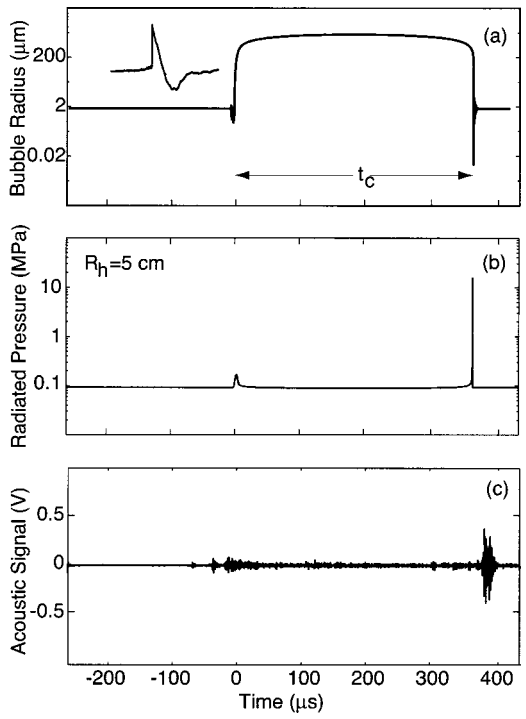

FIG. 2. (a) A (*time domain*) lithotripter pulse shown in the inset causes a preexisting bubble to undergo inertial cavitation, calculated here using the Gilmore equation. (b) The corresponding acoustic radiation pressure amplitude calculated from the curve in (a) at a distance of $R_h = 5$ cm from the bubble. (c) The measured time interval between compression and collapse agrees well with calculations. The calculated time interval is matched to the data by varying the pressure amplitude. (Courtesy of M. Bailey.)

II. THEORY

In the following subsections we describe our model for simulating radial bubble pulsations in SWL fields. We use a modified Rayleigh–Plesset bubble dynamics equation of motion, and incorporate mass and heat transfer across the bubble boundary, as well as chemical reactions. The model is based on applications to sonoluminescence (SL) bubbles.

A. Lithotripter pulse (the bubble driver)

For an electrohydraulic lithotripter, a high-voltage spark discharge at F1 (see Fig. 1) creates an underwater explosion, resulting in a finite amplitude, spherically diverging pressure wave. The form of the pressure wave includes a fast rise-time, high-amplitude compressive pulse, followed by a relatively long, lower amplitude rarefaction. A portion of the wave impinges on the ellipsoidal reflector, reflects, and focuses at F2. Initially, simulations of the SWL pulse were modeled as[22]

$$p(t) = 2p_a e^{-\alpha t}\cos(\omega t + \pi/3), \tag{1}$$

where p_a is the peak positive pressure, $\alpha = 9.1\times10^5$ is the decay constant and $\omega = 2\pi f$ ($f = 83.3$ kHz). However, subsequent Polyvinylidene fluoride (PVDF) hydrophone measurements have indicated that the negative portion of the waveform lasts longer than the model waveform. Furthermore, fiber-optic hydrophone studies have shown that the negative portion of the wave form lasts longer than PVDF hydrophone measurements, possibly due to the better adhesion of water to the glass fiber tip.[23,24] It can be argued that PVDF measurements of the wave form should be artificially extended to better match the fiber-optic measurements, rather than simply scale the pressure amplitude of the wave form.[17] Therefore, both measurements of the pressure field in our lithotripter and our simulations have artificially extended tails. In the simulations, we take $\alpha = 3.5\times10^5$ and $f = 50.0$ kHz. The temporal profile of the model and extended

wave forms can be seen in Fig. 3. The finite rise-time of the SWL pulse[22] is neglected since it is not important for bubble growth.

B. Bubble dynamics

This section will outline the derivation of the bubble dynamics model. More complete derivations have appeared elsewhere so interested readers should consult the references for details and justification of assumptions. We will discuss the model for the liquid dynamics, the gas dynamics, the boundary fluxes, as well as the spherical shape. The violent nonlinear oscillation of a bubble subjected to a variable pressure field is formally described by the coupling of the compressible Navier–Stokes equations in the liquid and the gas. Fortunately, the equations can be simplified and still describe the bubble dynamics accurately.

1. The dynamics of the liquid

If one assumes that the liquid surrounding a bubble is incompressible (or only mildly compressible) the Navier–Stokes equations of the liquid may be reduced to a nonlinear ordinary differential equation (ODE) for the bubble radius. This equation, typically known as the Rayleigh–Plesset equation (RPE), has various versions and derivations in the literature.[25] The form we use, which accounts for liquid compressibility, is given as[26,27]

$$\rho_L(\ddot{R}+\tfrac{3}{2}\dot{R}^2)=(P_b-P_\infty-P_F)+R\dot{P}/c_L, \tag{2}$$

where R is the bubble radius, ρ_L is the liquid density, P_∞ is the ambient pressure, P_F is the variable pressure due to the acoustic forcing, c_L is the speed of sound in the liquid, P_b is the pressure at the bubble wall in the liquid, and dots denote derivatives with respect to time. The pressure at the bubble wall is related to the internal gas pressure, P_g, by

$$P_b=P_g-\frac{2\sigma}{R}-4\mu\frac{\dot{R}}{R}, \tag{3}$$

where σ is the surface tension and μ is the liquid viscosity.

2. The dynamics of the gas

To close the Rayleigh–Plesset equation one must have an expression for the gas pressure in the bubble. The most basic simplification is to assume that the gas is obeying a polytropic law and that the pressure inside the bubble is spatially uniform. Under these assumptions the pressure is simply related to the bubble volume and the RPE is closed by the expression

$$P_g(t)=P_0\left(\frac{R_0}{R(t)}\right)^{3\gamma}. \tag{4}$$

The polytropic assumption is not appropriate for the violent phenomena that we will investigate in the current work, thus we will adopt a different approach.

Formally, the Navier–Stokes equations for the gas can be solved to obtain the gas pressure at the bubble wall; this was done in recent simulations[28] of the gas–vapor mixture which accounted for heat transfer, mass transfer, phase change, and chemical reactions. While it was shown that taking these details into account had important consequences for precisely understanding the state of the gas in violent cavitation phenomena, the basic physics of the radial dynamics can be captured with simpler models.[29–31]

To derive the average model, we start with the complete Navier–Stokes equations for a multi-species, reacting gas.[32] We will also assume that the pressure inside the bubble is spatially uniform. Despite the fact that the Mach number of the bubble wall can be very large, it was recently shown analytically that the pressure inside the bubble remains quite uniform for most of the cycle.[33] Pressure nonuniformities only exist when the bubble wall undergoes extreme acceleration, as when the collapse is halted and reversed. Even in violent collapses (using SL as a test case) where the pressure field has significant nonuniformities around the time of collapse, this variation does not influence the radial dynamics.

If we assume an ideal gas equation of state and ideal mixture rules it is straightforward to derive an ODE for the pressure in the bubble with the unknowns being the fluxes of heat and mass across the interface. Because this (or similar) results have appeared elsewhere[29–31] we present only the result

$$\dot{P}_g=P_g\gamma\left[\frac{\dot{n}}{n}-\frac{3\dot{R}}{R}\right]-(\gamma-1)\left[\sum\Gamma_iH_i-k\frac{3}{R}\frac{dT}{dr}\right], \tag{5}$$

where γ is the ratio of specific heats, n is the total number of moles of gas and vapor, Γ_i is the volumetric rate of production–destruction due to chemical reactions, H_i is the partial molar enthalpy of species i (the sum is taken over all species), k is the thermal conductivity of the gas, and dT/dr is the temperature gradient at the bubble wall.

One must also consider the total conservation of mass for the bubble. The rate of change in the number of moles of each $\dot{n}_i$ species is given by the rate of chemical production–destruction and flux due to either the phase change of the liquid at the bubble interface or the flux due to dissolved gas diffusion, n_i''. The expression is

$$\dot{n}_i=n_i''A+\Gamma_iV, \tag{6}$$

where A is the bubble surface area and V is the bubble volume. The volumetric rate of chemical production Γ_i is found by coupling the gas dynamic equations to a standard chemical kinetics reaction mechanism: This step is not necessary unless one is interested in the chemical output from the bubbles.

Coupling of bubble dynamics to the chemical reaction mechanism (by computing Γ_i) is outlined in several references.[34–36] The reaction mechanism we use in this work accounts for reactions of oxygen, nitrogen, water, and argon with 70 forward and reverse reactions with 19 different species. Again, this chemical coupling only matters when one is interested in the chemical output of a collapsing bubble, which will be presented later.

3. Models of the boundary flux

To solve the pressure and mass equations above, we need expressions for the flux of heat and mass at the boundary (dT/dr and n_i''). One simple method is based on compe-

tition of time scales.[36] When the bubble is moving rapidly compared to the time for heat diffusion out of the bubble, the bubble is assumed to behave adiabatically ($dT/dr=0$). When the bubble is moving slowly compared to heat diffusion, the bubble is assumed isothermal.

Toegel *et al.*[30] proposed a similar model giving an approximate form for the fluxes of heat and mass based on scaling arguments for a boundary layer. We adopt this model here as it provides physically realistic heat loss, which is important for modeling thermal damping. The temperature gradient is estimated as

$$\frac{dT}{dr}=\frac{T-T_\infty}{\delta}, \tag{7}$$

where the boundary layer thickness is given as $\delta=\sqrt{t_T\alpha}$, α is the thermal diffusivity of the multispecies gas, and the time scale for temperature changes is given as $t_T=R/3(\gamma-1)\dot{R}$. The thickness of the thermal boundary layer is not allowed to grow beyond the radius of the bubble. Note that since the thermal diffusivity α is proportional to $1/\rho$, the thermal boundary layer thickness scales as $\sqrt{R^4/\dot{R}}$, so that the boundary layer can be quite thin when the radius is small and the bubble is moving rapidly.

An approximation for the flux of vapor out of the bubble can be derived in a similar manner. The mass flux is given as the minimum of the rate of phase change from kinetic theory and the rate limited by inter-species mass diffusion. The flux of vapor out of the bubble is given as

$$n_i''=\min\left(D\frac{n-n_{\mathrm{eq}}}{V\delta},n_{\mathrm{evap}}''\right), \tag{8}$$

where n_{eq} is the number of moles of vapor in the bubble at equilibrium, and n_{evap}'' is the evaporative flux from kinetic theory. The boundary layer thickness, $\delta=\sqrt{t_N D}$, is defined with the mass diffusion coefficient, D and the time scale for the change in mole numbers $t_N=R/3\dot{R}$. Justification for these flux models can be found in the references.[29,30,36]

Expressions for the flux for dissolved gas species is given in detail by Fyrillas and Szeri.[37] These equations are applied to compute the rate of change of the number of moles of dissolved gas as the volume of the bubble changes.

4. Spherical stability

Due to the violent collapse, one must determine if the assumption of spherical symmetry of the bubble is justified. The spherical stability of bubbles has been analyzed by various authors and will not be repeated here.[38–40] Nonspherical perturbations grow on the collapse due to the acceleration of a heavy fluid into a light one. The afterbounces couple to the nonspherical oscillations causing parametric instability. Linear stability analysis can accurately predict the growth of nonspherical modes; this analysis has proved to be quite accurate even in the violent collapses found in single-bubble sonoluminescence (SBSL). We simply apply the analysis of the Rayleigh–Taylor instability found in the literature[39,40] and stop the calculation when the amplitudes on nonspherical modes grows to the order of magnitude of the bubble size.

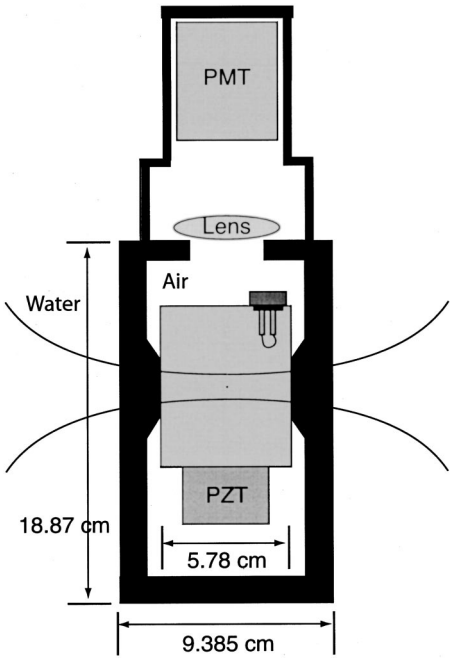

FIG. 4. Underwater levitation system used to place a single bubble at the focus of the lithotripter.

III. EXPERIMENT

All experiments were performed in a research electrohydraulic shock wave lithotripter,[13] modeled after the Dornier HM3, the most widely used clinical lithotripter in the United States.[41] Detailed characterization of the acoustic field for this lithotripter is not described here, but can be found elsewhere.[13,17] An example of the PVDF-measured wave form at the center of the 6 cm long by 1 cm diameter focus is shown in Fig. 3. For all experiments, the sparker voltage was set to 21 kV.

A. Single-bubble apparatus

Bubble response experiments were carried out in a specially designed underwater levitation chamber. Bubble levitation is a well-known technique that uses an acoustic standing wave to generate a time-averaged acoustic radiation force on the bubble that opposes the buoyancy force. With sufficient pressure amplitude, a bubble can be levitated at a pressure node or antinode, depending on the size of the bubble.[42,43] For our studies, bubbles smaller than resonance size were levitated, and thus they were held at the pressure antinode.

The underwater levitation chamber (Fig. 4) is almost completely surrounded by air, which provides good boundaries that reinforce a standing wave structure. However, a portion of two opposing walls of the chamber are coupled directly to the surrounding water tank in order to allow the shock wave to pass through relatively unimpeded (amplitude decreases by ≈5%). These walls are made of black Noryl polyphenylene oxide (PPO) plastic (specific gravity ≈1.06,

sound speed ≈2293 m/s). The outer enclosure houses the optical detection system, and provides support for the bubble levitation chamber. Two sides of the chamber are transparent to allow laser illumination. The bottom-mounted PZT excitation transducer is used to generate the standing wave in the water-filled chamber ($f_0 \approx 23$ kHz). Fluid ports (not shown) are incorporated to allow filling and draining of water.

Because the chamber is completely closed to its surroundings, a nichrome wire inserted into the chamber is used to generate bubbles.[44] We also partially degas (≈100 Torr) the levitation chamber water. Degassing serves two purposes. First, by removing most of the air from the water, the lithotripter pulse will not nucleate cavitation bubbles on its own. We verified this several times during the course of the experiment; sonoluminescence and acoustic signals were observed only when a bubble was levitated.

Second, we want to perform experiments on bubbles whose initial size is on the order of microns, not orders of magnitude larger. The initial creation of a bubble typically produces a larger-than-desired bubble, so that degassing serves as a means to decrease the bubble size through outward diffusion. Towards this end, we standardized our technique so that bubble dissolution lasted about 20–30 s. We then measured the bubble size in the submerged chamber using back-light imaging, and generated a calibration curve of size vs time. During an experiment, we fired the lithotripter when the bubble radius was expected to be less than 10–20 μm. Although bubble dynamics calculations indicate that the initial bubble radius is not important with respect to the overall growth and collapse sequence, one might expect that very large bubbles would experience asymmetries from the SWL pulse. We, therefore, tried to keep the initial bubble size small.

The bubble was aligned with the SWL pulse using laser illumination (≈2 to 3 mm beam waist) of the predetermined SWL focus. The levitation chamber positioned the bubble within the beam using a three-dimensional (3D) translation system. This same laser (a 0.5 mW HeNe source) also was used as the light scattering source, directed perpendicularly to the SWL pulse propagation direction. The light scattered from the bubble was focused onto a photomultiplier tube (PMT; Thorn EMI 9956KB, 12 ns response) using a 5 cm-diameter bi-convex lens mounted near the top of the enclosure. The output of the PMT was terminated into the 50 ohm impedance of an oscilloscope (Lecroy LC334 AL, 500 MHz), which was triggered with the SWL spark discharge.

B. Light-scattering

Originally used to size stationary bubbles in water[45–48] and to quantify radial instabilities in water,[49] light-scattering techniques have been refined to measure nonlinear pulsations of bubbles,[50] including the highly nonlinear oscillations of sonoluminescing bubbles.[51–53] The overwhelming success of this technique in measuring bubble oscillations—especially with respect to sonoluminescing bubbles—suggests that this technique can be applied to measuring bubbles in SWL.

The mathematics of light scattering from spherical bubbles is formally described by Mie scattering theory.[54] The features associated with Mie scattering can be complicated, as shown in Fig. 5(a). Here we assume an incident, linearly polarized ($\lambda = 632$ nm) plane wave scattering off a homogeneous 20 μm radius bubble in water (index of refraction ratio of water to air $n = 1.332$). The scattered intensity depends on bubble size, as well as scattering angle. The intensity generally decreases with increasing angle, and contains substantial fine oscillatory structure. This fine structure is smoothed out if light is collected over a relatively large angle. For example, collecting the light over an angular range that spans 10° results in the solid curve of Fig. 5(a). We also show as a comparison the scattered light intensity in the geometrical optics limit.[55]

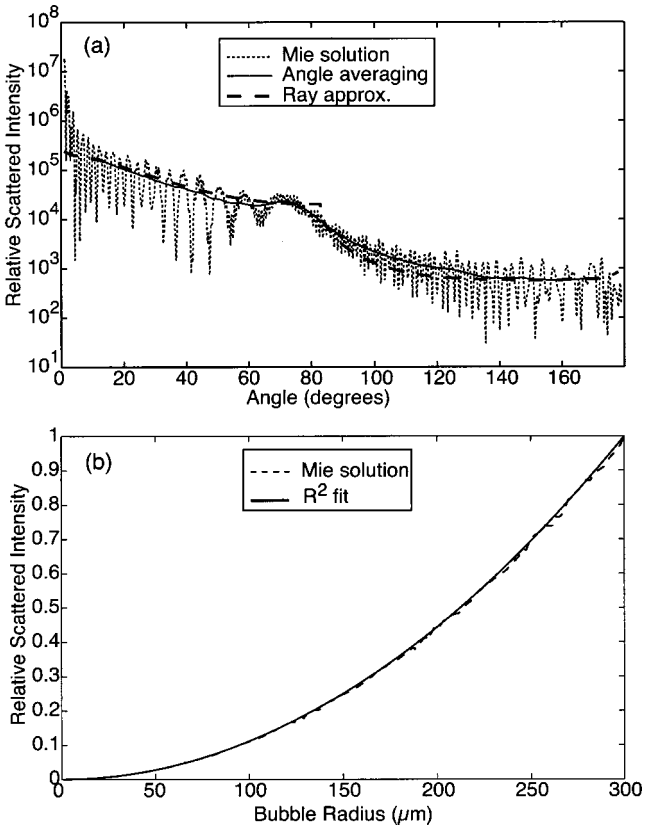

FIG. 5. (a) Mie scattered intensity for a 20 μm radius bubble vs detection angle. Finite angle collection and geometrical optics approximation curves are also shown. (b) Comparison of Mie scattered intensity to geometrical optics approximation vs bubble size.

In the experiments, we collected light spanning the range 64–96°, similar to what is used in sonoluminescence experiments.[52,53] This range is a compromise that provides a relatively good signal–noise ratio. The Mie solution vs radius for small bubbles, averaged over this finite angular range, is shown in Fig. 5(b). The scattered intensity follows the geometrical optics approximation ($I \propto R^2$) even for relatively small bubbles. Because SWL-generated bubbles spend most of the time at relatively large sizes, we can use the much simpler geometrical optics approximation to relate the scattered intensity to bubble size. Thus, for our experiments we take $R \propto \sqrt{I - I_0}$, where I_0 is the background light intensity. The proportionality constant is determined by single-

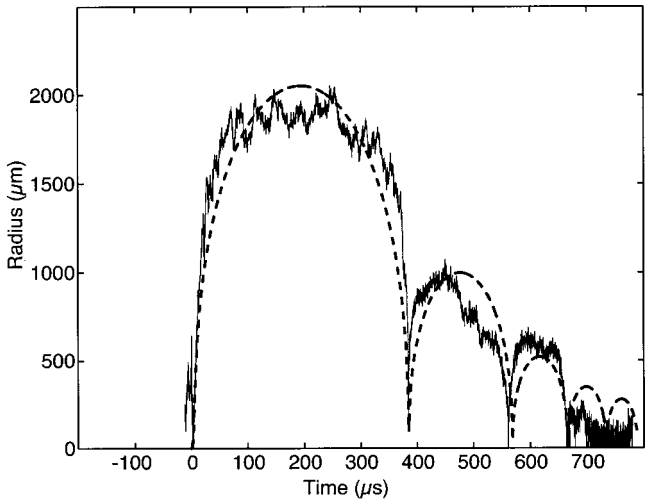

FIG. 6. Experimental and simulated radial dynamics from an SWL pulse. The fitted pressure amplitude is 33 MPa. The bubble was determined to be spherically unstable when the calculation ends.

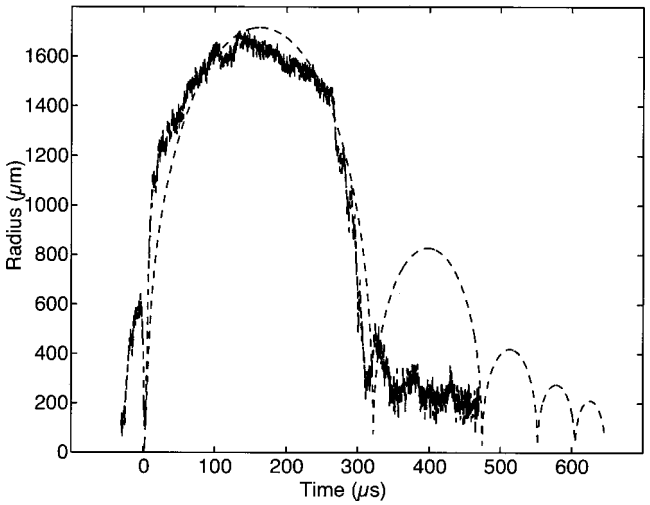

FIG. 7. Light scattered signal from a bubble in a cavitation field. The model ($P_a = 25.5$ MPa) fits the main growth and collapse sequence, but there are no large afterbounces observed. A bubble in the cavitation field will likely collapse nonspherically due to bubble–bubble interactions.

parameter (pressure amplitude) fitting of the data to the calculated $R(t)$ curve.

Finally we remark that the light scattered intensity is presumed to be from spherical bubbles, though it is probable that some bubbles undergo nonspherical pulsations. Although mathematical solutions exist for spheroidal particles,[56,57] we are unaware of solutions that might involve liquid jetting, capillary waves, etc. We confine ourselves to this study only to spherical dynamics. However, it is possible to use light scattering to record bubble instabilities and nonspherical oscillations. Hornsburgh[49] used light scattering (into two separate photodiodes) to determine the threshold for bubble instabilities, while Matula and Crum,[53] using light-scattering and direct imaging together, recorded light scattered signals that apparently correspond to quadrupole oscillations.

C. Data

An example of data obtained from the experiments is shown in Fig. 6. The model is fit to experiments by varying the pressure amplitude to match the experimentally measured time interval between compression and first collapse. The simulated initial bubble radius was $R_0 = 4.5$ μm. The initial bubble size does not play a large role in the maximum bubble size attained, nor in the afterbounces as the initial gas is overwhelmed by the vapor that evaporates into the bubble (this will be explained further below). The pressure pulse parameters were taken to be those in Fig. 3, and the liquid was water at 298 K degassed with air down to 100 Torr.

In Fig. 6 the bubble grows to almost 2 mm before undergoing an inertially dominated collapse about 400 μs later. The bubble then rebounds several times. It is unclear whether or not the bubble remains intact throughout, or if it fragments and then reforms during the rebound. The calculation stops when the model predicts that the bubble has gone spherically unstable. The model and the data indicate that the bubble apparently survives the inertially dominated collapse. The afterbounce intervals are much longer than predicted by the Gilmore model, and decrease with each afterbounce: This effect will be explained shortly.

We were also able to observe individual bubble dynamics from a cavitation cloud generated by an SWL pulse. Here we used the same single-bubble levitation chamber, but did not degas the water prior to the experiment. A very typical result of the light-scattered intensity from such a bubble is shown in Fig. 7. Although the main growth and collapse sequence agrees well with the model, we did not observe the large afterbounces that are normally observed from the single levitated bubble. Of the very many data sets we obtained (Fig. 7 is very typical) we *rarely* observed afterbounces similar to those shown in Fig. 6. One possible explanation is that the initial bubble was adjacent to the laser beam path, and not inside it. Then, upon expansion the bubble intersected the beam, resulting in an increase in light scattering, while the subsequent afterbounces were again outside the beam path. Other likely possibilities include bubble–bubble interactions that result in nonspherical collapses, causing the bubble to disintegrate during the collapse, or that adjacent bubbles coalesce, resulting in a soft, cushioned collapse. If nearby bubbles are illuminated, we probably would not be able to distinguish the bubbles, and coalescence would not be observed.

We wish to emphasize that Figs. 6 and 7, although typical, do not encompass all the different signals we have observed. Many signals show qualitatively similar behavior, but vary greatly in the quantitative nature of the collapse time, amplitude, symmetry during expansion and collapse, number of afterbounces, etc. High-speed photographs of cavitation clouds due to shock-wave lithotripsy also show a great variety of bubble behavior.[19] It is somewhat surprising that evidence of single bubble oscillations in a cavitation cloud (Fig. 7) can even be observed with laser scattering, given the apparent high density of bubbles observed with high-speed photographs. Our results suggest that the separation distance between neighboring bubbles can be larger than 1 to 2 mm.

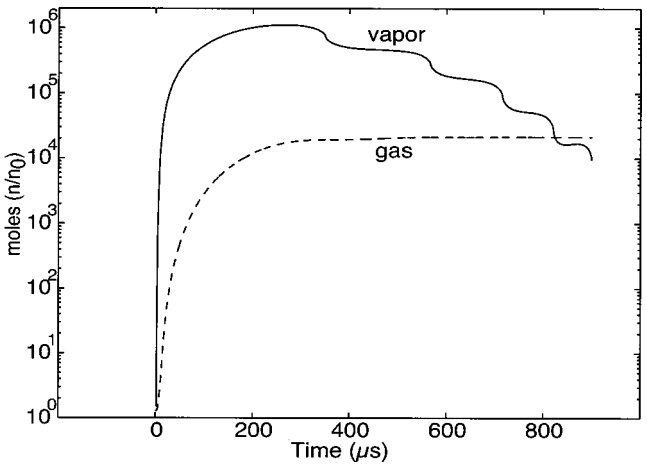

FIG. 8. Number of moles of gas (air) and water vapor contained in the bubble over the life of the oscillations, normalized by the number of moles originally in the bubble. The parameters are the same as those used in Fig. 6.

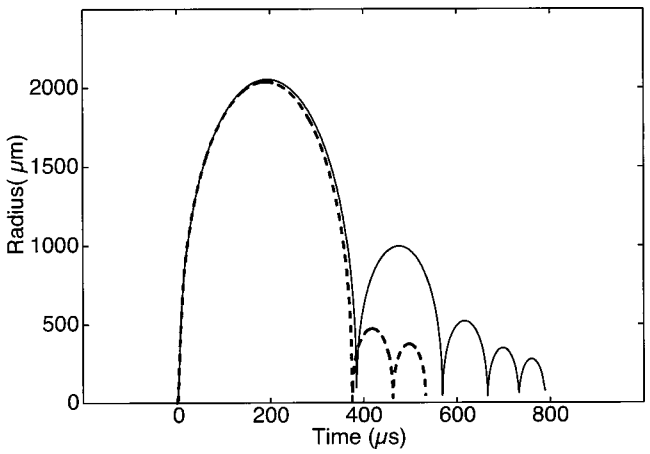

FIG. 9. Comparison of model with (solid curve) and without (dashed curve) water vapor taken into account. The afterbounces are much smaller when water vapor is neglected because the total mass inside the bubble is much smaller (see Fig. 8).

IV. DISCUSSION

Although our direct measurements of bubble oscillations in SWL are not completely unexpected, these studies have revealed several issues that have heretofore been neglected. Most importantly, vapor trapping softens the inertial collapse, leading to large afterbounces. In addition, we discuss below the possibility of bubble translation due to the acoustic radiation force. We conclude with a discussion of the relevance to multibubble cavitation fields that are normally generated in SWL.

A. Importance of water vapor, and limitations

While most models of bubble dynamics in SWL include diffusion of dissolved gas, we find that gas diffusion is secondary to vapor trapping. In Fig. 8 we show the number of moles of gas and vapor inside the bubble for the same conditions shown in Fig. 6. Vapor comprises the majority of the bubble contents throughout the growth phase, and over several afterbounces. The physics of the vapor trapping mechanism is discussed in the references section[29] in detail. Essentially, the collapse becomes so rapid that there is insufficient time for vapor deep in the bubble interior to escape.

Significant dissolved gas diffusion does occur as seen by the rapid growth in the amount of air in the bubble during the expansion. This growth in the dissolved gas overwhelms the amount of gas that was initially in the bubble: This answers the question of why the initial bubble radius is not important for fitting the experimental radial dynamics. In Fig. 9 we show the change in radial dynamics if vapor is neglected: The afterbounces are of smaller amplitude and higher frequency.

The model presented here is based on approximations for the heat and mass transfer out of the bubble. The boundary layer approximation, while physically relevant, is only based upon scaling arguments. There is no reason that an order unity scale factor cannot be included in the definition of the transport boundary layer thickness in Eqs. (7) and (8). The difference in the radial dynamics with a prefactor of 1, 2, and 4 added to the boundary layer thickness is shown in Fig. 10 (note that in previous figures no prefactor was used). Because we do not use a prefactor, we see clearly that the model is very sensitive to vapor trapping: less is trapped when the boundary layer is made thinner. Because the bubble is composed primarily of vapor the amount trapped by collapse controls the dynamics of the afterbounces. This limitation and sensitivity of the model should be understood.

B. Acoustic radiation force on bubble

An immediate concern prior to our experiments was whether or not the levitated bubble would experience large acoustic radiation forces from the SWL pulse, causing it to translate within, or even out of the laser beam. The translational equation of motion for the bubble, assuming it remains spherical, can be calculated from[58]

$$m_b \dot{U}_b = -V\nabla P_a - \frac{1}{2}\rho_l \frac{d}{dt}[VU_r] - \frac{1}{2}\rho_l U_r^2 A C_d . \qquad (9)$$

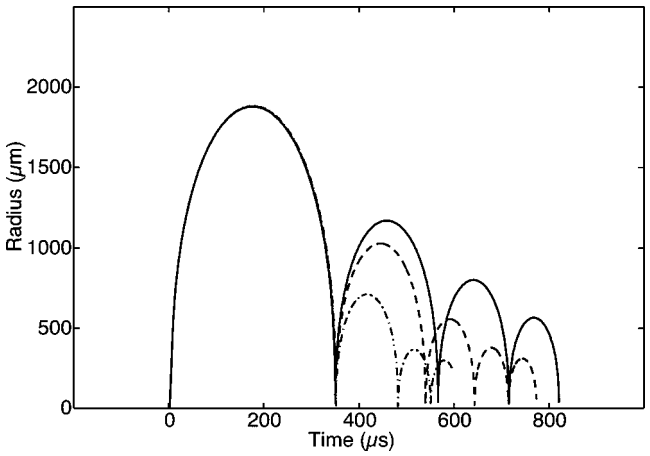

FIG. 10. Influence of the scaling law for mass transport of vapor within the bubble on the strength of the afterbounces. The dynamics are quite sensitive to the exact expression for the mass flux. The results show the effect of a scaling factor of 1 (solid), 2 (dashed), and 4 (dash–dot) in the term for the boundary layer thickness.

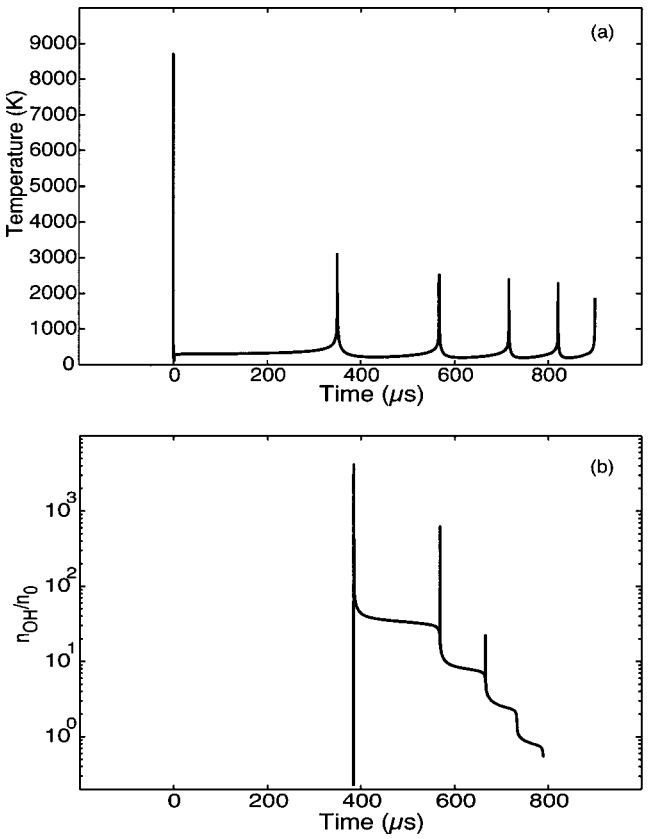

FIG. 11. Temperature (a) and OH radical production (b) for the same parameters used in Fig. 6. The temperature peaks in the forced compression because the bubble contains very little water vapor at that time.

The three terms on the right are the acoustic radiation force, the added mass force, and the drag force, respectively. Buoyancy is neglected here. The parameters include the mass of the bubble $m_b = \rho_g V$, ρ_g is the gas density, $A = \pi R^2$ is the projected area of the bubble, and C_d is the drag coefficient. A Stokes drag law is assumed here for simplicity; thus $C_d = 24/\mathrm{Re}$, where the Reynolds number $\mathrm{Re} = (2\rho_l/\mu)U_r R$, μ is the absolute shear viscosity, and $U_r = U_b - U_l$, where U_l is the velocity of the liquid.

Calculations suggest that the translational motion of the bubble is negligible compared to the beam diameter.[59] Nevertheless, we attempted to measure the translational displacement by narrowing the laser beam with a lens to ~ 0.5 mm, positioning the bubble adjacent to the beam, on the near side of the SWL spark, and measuring the scattered light intensity as the bubble translated through the beam path. If successful, we would expect to observe an increase in the scattered light intensity as the bubble entered the beam path, followed by a decrease in intensity as the bubble exited the beam path. We observed no such displacement signals. Bubbles placed near the far edge of the laser beam (with respect to the sparker unit) also showed no evidence of translation.

C. Thermal and chemical effects

The model used for this work allows for predictions of the temperature of the bubble collapse and the amount of OH radicals produced. The thermal and chemical activity of the bubble is shown in Fig. 11. We see that the initial shock compresses the bubble and a very high temperature is achieved. Due to the thinness of the shock front compared to the bubble radius, the bubble will not be forced spherically when the initial shock impacts the bubble, therefore this temperature is likely to be unphysical. Despite the high temperatures, there are few OH radicals produced in the forced compression as the bubble is nearly a pure air bubble; vapor provides the fuel for production of OH radicals.

On the free collapse, the temperature inside the bubble reaches $\sim$3000 K. Significant OH radical production occurs from this heating of the nearly pure vapor bubble. We see that the OH production slowly decays with spurts of OH production and destruction in subsequent afterbounces: similar behavior has been predicted in sonoluminescence.

D. Relevance to multibubble cavitation

The model thus far has provided good agreement with the single bubble cavitation experiments, but this is clearly very different than the behavior of multibubble cavitation. In Fig. 7 we show our fit of the model to the multibubble data, showing agreement with the main growth and collapse sequence, but not in the dynamics of the afterbounces. While the model presented in this paper is clearly not directly applicable to predicting precise dynamics and behavior of multibubble fields (with associated nonspherical pulsations, coalescence, etc.), the model nevertheless is very useful to lithotripsy. The single bubble model can be thought of as a limiting case. For example, if one wants to assess the potential biochemical effects of radicals produced from cavitation this model could provide an upper limit: A nonspherical collapse would not get as hot and produce fewer radicals. Bubble fragmentation would also serve to limit radical production. If the radical production from this model is not significant for cell and tissue damage, then the effect can be neglected.

V. CONCLUSION

Direct measurements of individual bubble dynamics from SWL have been performed for the first time. It was found that simulations of single bubble dynamics are in agreement with the data, provided vapor trapping is taken into account. Vapor trapping dramatically influences the hot-spot conditions within the bubble, limiting the temperature that can be achieved. Vapor-trapping also provides a cushion that causes the bubble to rebound to much greater amplitudes than previously thought. This cushioning may prevent the bubble from catastrophic disintegration upon collapse. Furthermore, the formation of hydroxyl radicals are closely tied to the amount of water vapor trapped in the bubble. The ability of this model to predict bubble motion in SWL (as well as in sonoluminescence) may be useful in calculations of the upper limit for radical production rates under various conditions.

ACKNOWLEDGMENTS

The authors wish to thank M. Bailey, D. Sokolov, and L. Crum for many fruitful discussions. T.M. was supported by

DARPA Grant No. N00014-99-1-0793 and P.H. was supported by NIH Grant No. DK43881. A.S. is supported by the U.S. National Science Foundation Program in Biomedical Engineering.

[1]S. A. V. Holmes and H. N. Whitfield, ''The current status of lithotripsy,'' Br. J. Urol. **68**, 337 (1991).
[2]C. Chaussy, W. Brendel, and E. Schmiedt, ''Extracorporeally induced destruction of kidney stones by shock waves,'' Lancet **2**, 1265 (1980).
[3]M. Delius and W. Brendel, ''A mechanism of gallstone destruction by extracorporeal shock waves,'' Naturwissenschaften **75**, 200 (1988).
[4]D. Howard and B. Sturtevant, ''*In vitro* study of the mechanical effects of shockwave lithotripsy,'' Ultrasound Med. Biol. **23**, 1107 (1997).
[5]M. Lokhandwalla and B. Sturtevant, ''Fracture mechanics model of stone comminution in ESWL and implications for tissue damage,'' Phys. Med. Biol. **45**, 1923 (2000).
[6]S. M. Gracewski, G. Dahake, Z. Ding *et al.*, ''Internal stress wave measurements in solids subjected to lithotripter pulses,'' J. Acoust. Soc. Am. **94**, 652 (1993).
[7]A. J. Coleman, J. E. Saunders, L. A. Crum *et al.*, ''Acoustic cavitation generated by an extracorporeal shockwave lithotripter,'' Ultrasound Med. Biol. **13**, 69 (1987).
[8]L. A. Crum, ''Cavitation microjets as a contributory mechanism for renal calculi disintegration in ESWL,'' J. Urology **140**, 1587 (1988).
[9]A. Vogel and W. Lauterborn, ''Acoustic transient generation by laser-produced cavitation bubbles near solid boundaries,'' J. Acoust. Soc. Am. **84**, 719 (1988).
[10]W. Eisenmenger, ''The mechanisms of stone fragmentation in ESWL,'' Ultrasound Med. Biol. **27**, 683 (2001).
[11]A. P. Evan and J. A. McAteer, in *Kidney Stones: Medical and Surgical Management*, edited by C. Pak, F. Coe, and G. M. Preminger (Taven, New York, 1996), pp. 549–570.
[12]A. J. Coleman, J. E. Saunders, R. C. Preston *et al.*, ''Pressure waveforms generated by a Dornier extra-corporeal shock-wave lithotripter,'' Ultrasound Med. Biol. **13**, 651 (1987).
[13]R. O. Cleveland, M. R. Bailey, N. Fineberg *et al.*, ''Design and characterization of a research electrohydraulic lithotripter patterned after the Dornier HM3,'' Rev. Sci. Instrum. **71**, 2514 (2000).
[14]A. J. Coleman, M. J. Choi, and J. E. Sanders, ''Detection of acoustic emission from cavitation in tissue during clinical extracorporeal lithotripsy,'' Ultrasound Med. Biol. **22**, 1079 (1996).
[15]A. J. Coleman, M. J. Choi, J. E. Saunders *et al.*, ''Acoustic emission and sonoluminescence due to cavitation at the beam focus of an electrohydraulic shock wave lithotripter,'' Ultrasound Med. Biol. **18**, 267 (1992).
[16]R. O. Cleveland, O. A. Sapozhnikov, M. R. Bailey *et al.*, ''A dual passive cavitation detector for localized detection of lithotripsy-induced cavitation in vitro,'' J. Acoust. Soc. Am. **107**, 1745 (2000).
[17]M. R. Bailey, D. T. Blackstock, R. O. Cleveland *et al.*, ''Comparison of electrohydraulic lithotripters with rigid and pressure-release ellipsoidal reflectors. II. Cavitation fields,'' J. Acoust. Soc. Am. **106**, 1149 (1999).
[18]T. Kodama and Y. Tomita, ''Cavitation bubble behavior and bubble-shock wave interaction near a gelatin surface as a study of *in vivo* bubble dynamics,'' Appl. Phys. B **70**, 139 (2000).
[19]P. Zhong, Y. Zhou, and S. Zhu, ''Dynamics of bubble oscillation in constrained media and mechanisms of vessel rupture in SWL,'' Ultrasound Med. Biol. **27**, 119 (2001).
[20]K. Jochle, J. Debus, W. J. Lorenz *et al.*, ''A new method of quantitative cavitation assessment in the field of a lithotripter,'' Ultrasound Med. Biol. **22**, 329 (1996).
[21]P. Huber, K. Jochle, and J. Debuss, ''Influence of shock wave pressure amplitude and pulse repetition frequency on the lifespan, size and number of transient cavities in the field of an electromagnetic lithotripter,'' Phys. Med. Biol. **43**, 3113 (1998).
[22]C. C. Church, ''A theoretical study of cavitation generated by an extracorporeal shock wave lithotripter,'' J. Acoust. Soc. Am. **86**, 215 (1989).
[23]J. Staudenraus and W. Eisenmenger, ''Fibre-optic probe hydrophone for ultrasonic and shock-wave measurements in water,'' Ultrasonics **31**, 267 (1993).
[24]C. Wurster, J. Staudenraus, and W. Eisenmenger, ''The fibre optic probe hydrophone,'' Nature (London) **2**, 941 (1994).
[25]A. Prosperetti and A. Lezzi, ''Bubble dynamics in a compressible liquid. I. First-order theory,'' J. Fluid Mech. **168**, 457 (1986).
[26]R. Lofstedt, K. Weninger, S. Putterman *et al.*, ''Sonoluminescing bubbles and mass diffusion,'' Phys. Rev. E **51**, 4400 (1995).
[27]S. Hilgenfeldt, M. P. Brenner, S. Grossmann *et al.*, ''Analysis of Rayleigh–Plesset dynamics for sonoluminescing bubbles,'' J. Fluid Mech. **365**, 171 (1998).
[28]B. D. Storey and A. J. Szeri, ''Mixture segregation within sonoluminescence bubbles,'' J. Fluid Mech. **396**, 203 (1999).
[29]B. D. Storey and A. J. Szeri, ''Water vapour, sonoluminescence and sonochemistry,'' Proc. R. Soc. London, Ser. A **456**, 1685 (2000).
[30]R. Toegel, B. Gompf, R. Pecha *et al.*, ''Does water vapor prevent upscaling sonoluminescence?'' Phys. Rev. Lett. **85**, 3165 (2000).
[31]A. Prosperetti, L. A. Crum, and K. W. Commander, ''Nonlinear bubble dynamics,'' J. Acoust. Soc. Am. **83**, 502 (1988).
[32]R. B. Bird, W. E. Stewart, and E. N. Lightfoot, *Transport Phenomena* (Wiley, New York, 1960).
[33]H. Lin, B. D. Storey, and A. J. Szeri, ''Inertially driven inhomogeneities in violently collapsing bubbles: The validity of the Rayleigh–Plesset equation,'' J. Fluid Mech. (to be published).
[34]C. Gong and D. P. Hart, ''Ultrasound induced cavitation and sonochemical yields,'' J. Acoust. Soc. Am. **104**, 2675 (1998).
[35]A. J. Colussi, L. K. Weavers, and M. R. Hoffmann, ''Chemical bubble dynamics and quantitative sonochemistry,'' J. Phys. Chem. A **102**, 6927 (1998).
[36]B. D. Storey and A. J. Szeri, ''A reduced model of cavitation physics for use in sonochemistry,'' Proc. R. Soc. London, Ser. A **457**, 1685 (2001).
[37]M. M. Fyrillas and A. J. Szeri, ''Dissolution or growth of soluble, spherical, oscillating bubbles,'' J. Fluid Mech. **277**, 381 (1994).
[38]M. S. Plesset, ''On the stability of fluid flows with spherical symmetry,'' J. Appl. Phys. **25**, 96 (1954).
[39]Y. Hao and A. Prosperetti, ''The effect of viscosity on the spherical stability of oscillating gas bubbles,'' Phys. Fluids **11**, 1309 (1999).
[40]S. Hilgenfeldt, D. Lohse, and M. P. Brenner, ''Phase diagrams for sonoluminescing bubbles,'' Phys. Fluids **8**, 2808 (1996).
[41]J. E. Lingeman, *New Developments in the Management of Urolithiasis* (Igaku-Shoin, New York, 1996).
[42]A. I. Eller, ''Force on a bubble in a standing acoustic wave,'' J. Acoust. Soc. Am. **43**, 170 (1968).
[43]T. J. Matula, S. M. Cordry, R. A. Roy *et al.*, ''Bjerknes force and bubble levitation under single-bubble sonoluminescence conditions,'' J. Acoust. Soc. Am. **102**, 1522 (1997).
[44]R. Hiller, K. Weninger, S. J. Putterman *et al.*, ''Effect of noble gas doping in single-bubble sonoluminescence,'' Science **266**, 248 (1994).
[45]P. L. Marston, ''Critical angle scattering by a bubble physical-optics approximation and observations,'' J. Opt. Soc. Am. **69**, 1205 (1979).
[46]D. L. Kingsbury and P. L. Marston, ''Mie scattering near the critical angle of bubbles in water,'' J. Opt. Soc. Am. **71**, 358 (1981).
[47]D. S. Langley and P. L. Marston, ''Critical-angle scattering of laser light from bubbles in water: Measurements, models, and application to sizing of bubbles,'' Appl. Opt. **23**, 1044 (1984).
[48]G. M. Hansen, ''Mie scattering as a technique for the sizing of air bubbles,'' Appl. Opt. **24**, 3214 (1985).
[49]S. D. Horsburgh, Ph.D. thesis, University of Mississippi, 1990.
[50]R. G. Holt and L. A. Crum, ''Mie scattering used to determine spherical bubble oscillations,'' Appl. Opt. **29**, 4182 (1990).
[51]D. F. Gaitan, Ph.D. thesis, University of Mississippi, 1990.
[52]B. P. Barber and S. J. Putterman, ''Light scattering measurements of the repetitive supersonic implosion of a sonoluminescing bubble,'' Phys. Rev. Lett. **69**, 3839 (1992).
[53]T. J. Matula, ''Inertial cavitation and single-bubble sonoluminescence,'' Philos. Trans. R. Soc. London, Ser. A **357**, 225 (1999).
[54]H. C. van de Hulst, *Light Scattering by Small Particles* (Dover, New York, 1981).
[55]G. E. Davis, ''Scattering of light by an air bubble in water,'' J. Opt. Soc. Am. **45**, 572 (1955).
[56]S. Asano, ''Light scattering properties of spheroidal particles,'' Appl. Opt. **18**, 712 (1979).
[57]S. Asano and G. Tamamoto, ''Light scattering by a spheroidal particle,'' Appl. Opt. **14**, 29 (1973).
[58]T. Watanabe and Y. Kukita, ''Translational and radial motions of a bubble in an acoustic standing wave field,'' Phys. Fluids A **5**, 2682 (1993).
[59]D. L. Sokolov, L. A. Crum, and M. R. Bailey, ''Use of a dual-pulse lithotripter to generate a localized and intensified cavitation field,'' J. Opt. Soc. Am. **110**, 1685 (2001).